https://doi.org/10.32604/zkg.2025.074711

ARTICLE

Study on erosion resistance and strength characteristics of basalt fiber sandstone cement stabilized macadam

Bin Zhang[1], Bin Zhao[1], Zhanli Zhang[2,*], Yongliang Liu[1], Tuo Huang[2,*] and Dabin Zhang[3]
[1]China Construction Infrastructure Corp., Ltd., Beijing, 100029, China
[2]National Engineering Laboratory of Highway Maintenance Technology, School of Transportation, Changsha University of Science & Technology, Changsha, 410114, China
[3]Guangxi GuiTong Engineering Management Group Co., Ltd., Nanning, 530001, China
*Corresponding Authors: Zhanli Zhang. Email: zhangzhanli@stu.csust.edu.cn; Tuo Huang. Email: ht@csust.edu.cn
Received: 16 October 2025; Accepted: 08 December 2025

ABSTRACT: Paving materials for semi-rigid base asphalt pavements in high-grade highways have traditionally employed high-quality intermediate to alkaline aggregates. Due to resource depletion, weakly acidic aggregates like sandstone are now increasingly used. However, cement-stabilized sandstone gravel is prone to shrinkage cracks and exhibits insufficient strength and erosion resistance. This study proposes incorporating basalt fiber to enhance its overall performance. The optimal mix parameters were determined through mechanical and shrinkage tests, resulting in a combination of 4% cement content with 1% basalt fiber of 18 mm length. This optimal mixture significantly improved performance: it reduced the dry shrinkage coefficient by 15.2% and the temperature shrinkage coefficient in the high-temperature range (40–30°C), moderate-temperature range (30–0°C), and low-temperature range (0 to –10°C) by 10.4%, 32.4%, and 14.1%, respectively. The fiber reinforcement increased the unconfined compressive strength, flexural tensile strength, and direct tensile strength by 8.86%, 27.47%, and 23.52%, and improved water stability by 42.89%. This study provides a technically feasible solution for highway construction in sandstone-rich areas, offering significant potential for resource substitution and cost savings. Optimizing fiber blending process can reduce material and transportation costs, improve the performance of the base material, and have engineering promotion value.

KEYWORDS: Basalt fiber; sandstone; cement stabilized gravel; mechanical properties

MATERIALS

1 Introduction

Cement-stabilized materials have become the preferred paving material for semi-rigid base asphalt pavement structures in high-grade highways due to their high strength [1], good slab integrity [1, 2], low deflection [3], strong load diffusion capacity, and low cost [3, 4]. Aggregates represent the most critical component of pavement materials such as cement-stabilized crushed stone or asphalt mixtures [5–7], and their quality directly affects road performance. However, the scarcity and high cost of high-quality aggregates, such as basalt, limestone, and diabase, have become increasingly prominent. Consequently, researchers have gradually turned their attention to seeking alternative materials. To date, studies have explored the feasibility of using construction waste [8, 9], slag [10], steel slag [11], feldspar powder (FP) [12], and sandstone [13] as cement-stabilized crushed stone aggregates, yielding numerous findings. Among these, sandstone aggregate, a by-product of mountain excavation, is characterized by dense texture, high hardness, and strong wear resistance. However, many studies have shown [14, 15] that, compared with conventional aggregates such as limestone and diabase, sandstone exhibits significant microstructural differences: it possesses higher porosity, stronger water absorption, and poorer water retention capacity. These properties result in an unstable cement hydration environment and a relatively loose interfacial transition zone (ITZ) structure, which in turn adversely affects the shrinkage performance, strength development, and long-term durability of the base material [16]. These microstructural characteristics also directly influence the interaction with fiber materials. The reinforcing effect of fibers is highly dependent on the surface characteristics of the aggregate, the pore structure, and the bonding performance at the fiber–matrix interface. For instance, in dense aggregates such as diabase, fibers mainly serve a bridging and crack-resistant function; in high-porosity sandstone, fibers may also form a spatial network within the pores, influencing the formation and development of hydration products and thereby affecting macroscopic properties.

In recent years, fiber-reinforcement technology has been increasingly applied in soil and cement-based materials. Heirani et al. [17] investigated the mechanism of polyurethane and waste tire textile fibers in synergistically stabilizing highly expansive clay, and found that fiber incorporation not only improves the compressive and tensile strength of the material, but also significantly enhances its toughness and crack resistance. Similarly, Pouramin et al. [18] examined the performance of composite-stabilized clay—comprising carbonized lime, electric furnace steel slag, and waste tire textile fibers—under freeze–thaw cycles. The results demonstrated that the introduction of fibers effectively improved the durability and microstructural integrity of the material. These studies provide important insights into the reinforcement mechanisms of fibers in high-porosity aggregates, particularly in terms of enhancing the interfacial transition zone and suppressing microcrack propagation.

Currently, many researchers focus on the use of external additives to enhance the overall performance of cement-stabilized crushed stone. Guo et al. [19] incorporated glass fiber—which offers economic benefits, ready availability, and effective toughening—into cement-stabilized crushed stone. They evaluated the improvement in softening and crack resistance through drying shrinkage tests, temperature shrinkage tests, flexural toughness tests, and fracture energy tests. The results demonstrate that glass fiber effectively reduces both the dry shrinkage and temperature shrinkage coefficients of cement-stabilized crushed stone, while also increasing the ultimate failure load. Zhao et al. [20] used polyvinyl alcohol fiber as an additive in cement-stabilized macadam, which improved both crack resistance and mechanical properties. Li et al. [21] introduced waste cooking oil (WCO) into cement-stabilized macadam, effectively reducing the dry shrinkage coefficient and enhancing fatigue cracking resistance. Furthermore, relevant studies [22–25] have indicated that basalt fiber can not only improve the anti-shrinkage performance and resistance to thermal cycle-induced cracking of cement-stabilized macadam but also significantly enhance its strength characteristics and erosion resistance. Therefore, the use of basalt fiber to improve the comprehensive performance of cement-stabilized macadam is of considerable research significance.

At present, most domestic research focuses on conventional aggregate systems. Studies on the fiber reinforcement mechanism in high-adsorption and high-porosity aggregates such as sandstone remain insufficient, particularly regarding the improvement of erosion resistance. Existing literature has yet to elucidate the specific mechanisms by which fibers enhance the sandstone–cement interface structure, regulate water migration, and improve erosion resistance. To address this research gap, this study proposes the incorporation of basalt fiber to improve its overall service performance. Firstly, the optimum cement dosage will be determined based on the 7-day unconfined compressive strength. Subsequently, the optimal fiber length and content will be identified through dry shrinkage and temperature shrinkage tests. Then, a series of experiments—including unconfined compression, direct tensile, and indirect tensile strength tests, as well as anti-erosion tests at different curing ages—will be conducted to evaluate the enhancing effect of basalt fiber on cement-stabilized sandstone gravel before and after its incorporation.

2 Materials and methods

2.1 Cement, basalt fiber and sandstone aggregates

In this study, P·O 42.5 ordinary Portland cement was used, with properties conforming to the requirements specified in the *Technical Rules for Construction of Highway Pavement Base* (JTG/T F20-2015) [26]. The technical indicators are presented in Table 1. The aggregates consisted of sandstone obtained from the Cangzhao Expressway in Guangxi. In accordance with the material classification criteria for heavy-traffic expressway base courses outlined in (JTG/T F20-2015) [26], four graded aggregates with sizes of 0–5 mm, 5–10 mm, 10–20 mm, and 20–30 mm were prepared using a combination of jaw crushing, cone crushing, and impact crushing processes. These aggregates exhibited appropriate specifications and favorable particle morphology, as shown in Figure 1. The test results of their technical indicators are provided in Tables 2 and 3. Basalt fiber with a diameter of 16 µm, supplied by Jiangsu Tianlong Company, was selected. The fibers appear golden brown in color, are environmentally benign, free of fluff, and show minimal splitting. The corresponding technical indicators are summarized in Table 4.

Table 1 Cement technical indicators

Cement	Stability (mm)	Initial Set (min)	Final Set (min)	Compressive Strength (MPa)		Break off Strength (MPa)	
				3 d	28 d	3 d	28 d
P·O 42.5	1.5	217	392	29.8	52.5	5.8	8.4
Technical requirement	≤5.0	≥180	360~600	≥17.0	≥42.5	≥4.0	≥6.5

(a) (b) (c) (d)

Figure 1 Aggregates after processing; (a) 20~30 mm; (b) 10~20 mm; (c) 5~10 mm; (d) 0~5 mm

Table 2 Technical indexes of coarse aggregate

Targets of Test	20~30 mm	10~20 mm	5~10 mm	Technical Requirement	Result Determination
Flat elongated particles content (%)	9.39	9.97	8.58	≤22	Qualification
Relative density of bulk volume (g/cm³)	2.72	2.71	2.69	—	—
Apparent density (g/cm³)	2.75	2.74	2.74	≥2.5	Qualification
Water absorption (%)	0.44	0.31	0.77	≤3.0	Qualification
Particle content below 0.075 mm (%)	1.00	0.80	0.20	≤2.0	Qualification
Crush value (%)	10.22			≤26	Qualification
Soft stone content (%)	1.17			≤5	Qualification

Table 3 Technical indexes of fine aggregate

Targets of Test	0~5 mm	Technical Requirement	Result Determination
Apparent density (g/cm³)	2.76	≥2.5	Qualification
Water absorption (%)	2.71	—	—
Particle content below 0.075 mm (%)	5.23	—	—
Plasticity index (%)	6.04	≤17	Qualification
Oganic content (%)	0.02	<2	Qualification
Sulfate content (%)	Shallow than the standard solution color	≤0.25	Qualification

Table 4 Technical indexes of basalt fiber

Targets of Test	Density (g/cm³)	Breaking Strength (MPa)	Breaking Elongation (%)	Elastic Modulus (MPa)	Water Content (%)	Combustible Matter Content (%)	Alkali Resistance (%)
Fiber properties	2.68	1723	2.70	8100	0.02	0.70	83

2.2 Specimen preparation and erosion resistance

To better simulate the compaction effect of heavy rollers on the construction site, cylindrical and beam specimens of cement-stabilized sandstone gravel were prepared using the vibration compaction method. The specimens had dimensions of ϕ 150 mm × 150 mm and 100 mm × 100 mm × 400 mm, respectively. The specimen preparation and curing process are shown in Figure 2.

In the experiment, a small amount of basalt fiber was incorporated using the "external mixing method," which had minimal influence on the optimum moisture content and maximum dry density of the mixture. To ensure uniform fiber dispersion, a staged mixing procedure commonly employed in engineering practice was adopted. The specific steps were as follows: first, the aggregates and fibers were dry-mixed in a mixer for 3 min to achieve initial fiber dispersion; then, water corresponding to 2% below the optimum moisture content was added, and wet mixing was conducted for 4 min. Subsequently, the mixture was sealed and allowed to soak for 2 h. After that, cement and the remaining 2% of water were added, followed

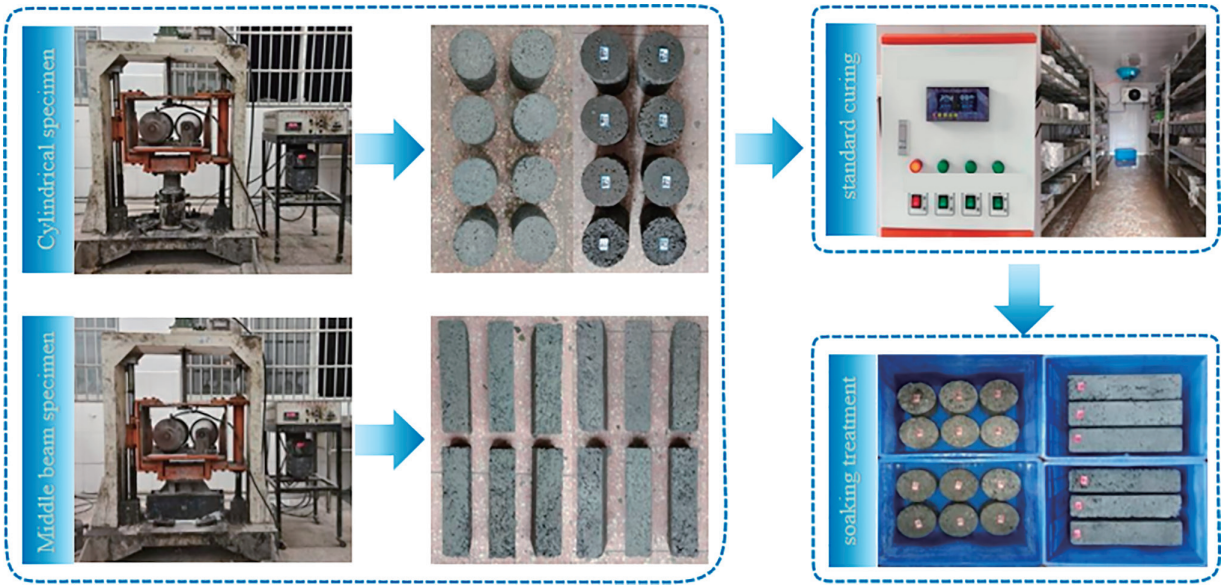

Figure 2 Specimen preparation and health preservation

by an additional 5 min of mixing. To effectively prevent fiber agglomeration, manual turning and rubbing were applied during both the wet mixing and final mixing stages. Using rubber-gloved hands, the mixture was gently rubbed with particular attention to visible fiber clusters. The cumulative rubbing time was controlled within 2 min. To evaluate the uniformity of fiber dispersion, random samples were extracted from different batches of the mixture after molding, and fiber distribution was assessed via CT scanning analysis. Fiber counts are presented in Figure 3. The calculated coefficients of variation were all less than 0.3, indicating that the process repeatability met the requirements. During compaction, the compaction coefficient was set to 98%, and a 2% mass loss compensation value was introduced. The inner wall of the mold and the base were coated with lubricating oil. The mixture was loaded into the mold in three layers, and vibration compaction was applied using a compaction instrument. Cylindrical specimens were vibrated for 120 s, while beam specimens were vibrated for 180 s. After molding, the specimens were demolded following a 2-h resting period, immediately sealed in plastic bags with the air expelled, and then placed in a standard curing room maintained at 20 ± 2°C with a relative humidity of ≥95%. Twenty-four hours prior to reaching the designated curing age, the specimens were transferred to a water tank at 20 ± 2°C for soaking.

2.3 Optimum moisture content and maximum dry density

In accordance with the gradation recommended for cement-stabilized macadam in the *Technical Rules for Construction of Highway Pavement Bases* (JTG/T F20-2015) [26], the C-B-3 skeleton-dense gradation type was adopted for the sandstone gravel mixture design, as illustrated in Figure 4.

According to the vibration compaction test method in *Test Specification for Inorganic Binder*

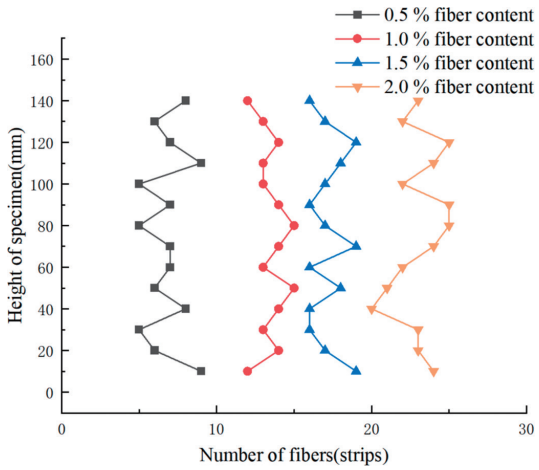

Figure 3 Fiber distribution map

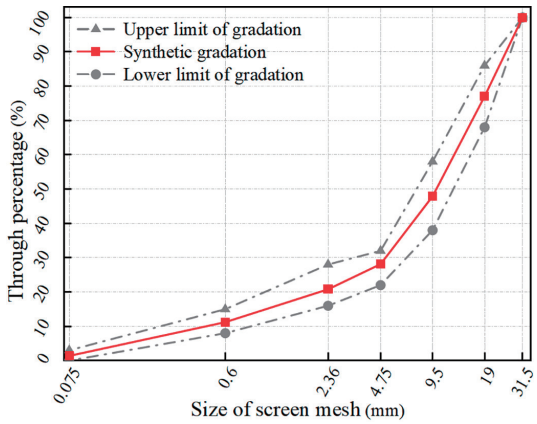

Figure 4 Gradation curve of cement stabilized sandstone gravel

Table 5 Compaction test to determine the optimum moisture content and maximum dry density

Index	Cement Dosage (%)				
	4.0	4.5	5.0	5.5	6.0
Optimum moisture content (%)	5.38	5.55	5.76	5.83	5.91
Maximum dry density (g/cm³)	2.3693	2.3907	2.4064	2.4253	2.4369

Stabilized Materials for Highway Engineering (JTG 3441-2024) [27], the compaction test was carried out on five different cement dosages, including 4.0%, 4.5%, 5.0%, 5.5% and 6.0%. The results are shown in Table 5.

2.4 Test method

To investigate the effect of basalt fiber on the performance of cement-stabilized sandstone macadam, subsequent tests were conducted in accordance with the *Test Methods of Materials Stabilized with Inorganic Binders for Highway Engineering* (JTG 3441-2024) [27]. To evaluate the influence of basalt fiber length and content on the shrinkage characteristics of cement-stabilized sandstone gravel and to determine the optimal fiber parameters for shrinkage resistance, fibers of four lengths (6 mm, 12 mm, 18 mm, and 24 mm) and four contents (0.5%, 1%, 1.5%, and 2%) were incorporated into the mixture at a fixed cement dosage of 4%. A control group without fiber was also prepared for comparison. Each experimental group consisted of six specimens: three for deformation measurement and three for determining the water loss rate. The drying shrinkage tests were performed in a climate-controlled chamber maintained at 20 ± 2°C and 60 ± 5% relative humidity. The specimen preparation and curing ages for the temperature shrinkage and drying shrinkage tests were identical. After curing, the specimens were oven-dried at 105 ± 1°C until constant mass was achieved, and their initial lengths were measured after cooling to room temperature. The test setup and procedures were consistent with those used in the drying shrinkage test. To evaluate the mechanical properties of the stabilized gravel, unconfined compressive strength tests were conducted using an MTS testing system. To ensure the reliability of the results, 13 parallel tests were performed for each group, and the average value was taken. The coefficient of variation (C_v) for each group was required to be ≤20%. Additionally, flexural tensile strength tests and direct tensile tests were carried out on the cement-stabilized sandstone gravel using the same MTS system, during which the maximum failure load P (N) was recorded. To evaluate the durability of the pavement, with reference to the specifications on the curing ages of cement-stabilized materials in the *Code for Design of Highway Asphalt Pavement* (JTG D50-2017) [28], φ 150 mm × 150 mm cylindrical specimens with standard curing ages of 7 d, 14 d, 28 d, 60 d, and 90 d were prepared. After 24 h of saturation, a dynamic water scour test was conducted under a peak impact force of 0.5 MPa and a scour frequency of 10 Hz, with a total test duration of 30 min.

3 Results and discussion

3.1 Determination of optimum cement dosage and basalt fiber length and content

3.1.1 Determination of good cement content

As shown in Figure 5, to determine the optimal cement content, the 7-day unconfined compressive strength test of cement stabilized sandstone gravel was carried out. The test results are shown in Figure 6.

Figure 5 Unconfined compressive strength test

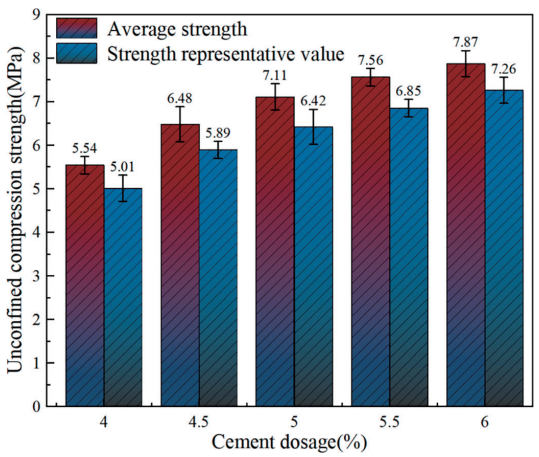

Figure 6 Effect of cement dosage on 7 d unconfined compressive strength

According to the test results, the compressive strength increases with higher cement dosage, which can be attributed to the synergistic effects of cement hydration activity and structural densification. As the cement content increases, the amount of hydration products rises, forming a dense cemented network. Simultaneously, the increased cement paste more fully coats the aggregates, fills the voids, and improves overall compactness. Furthermore, higher cement content optimizes the mixture gradation, enhancing the interlocking effect and stress transfer efficiency between aggregates. According to the *Code for Design of Highway Asphalt Pavement* (JTG D50-2017) [28], the representative value of the 7-day unconfined compressive strength for cement-stabilized materials should be in the range of 4.0–6.0 MPa when used in expressway cement-stabilized macadam bases under heavy traffic loads. Based on the test results, a cement dosage greater than 5% exceeds the specification limits. At a cement dosage of 4.5%, the compressive strength reaches 5.89 MPa, closing to the upper limit specified. With reference to local engineering experience, and to mitigate early cracking of the cement-stabilized sandstone gravel base and reduce project costs, a cement dosage of 4% was selected for subsequent research in this study.

3.1.2 Determination of optimum fiber length and dosage

The optimum fiber length and content were determined based on the dry temperature shrinkage coefficient. With reference to previous research [29] and engineering experience, a broad range of basalt fiber lengths (6–24 mm) and contents (mass fraction of 0.5%–2%) were selected. In accordance with the standard test methods, drying shrinkage and temperature shrinkage tests were conducted on cement-stabilized sandstone gravel with varying basalt fiber lengths and contents. The relevant calculation formulas for the drying shrinkage coefficient are provided in Equations (1)–(4). The test results are presented in Figure 7.

$$w_i = \frac{m_i - m_{i+1}}{m_p} \quad (1)$$

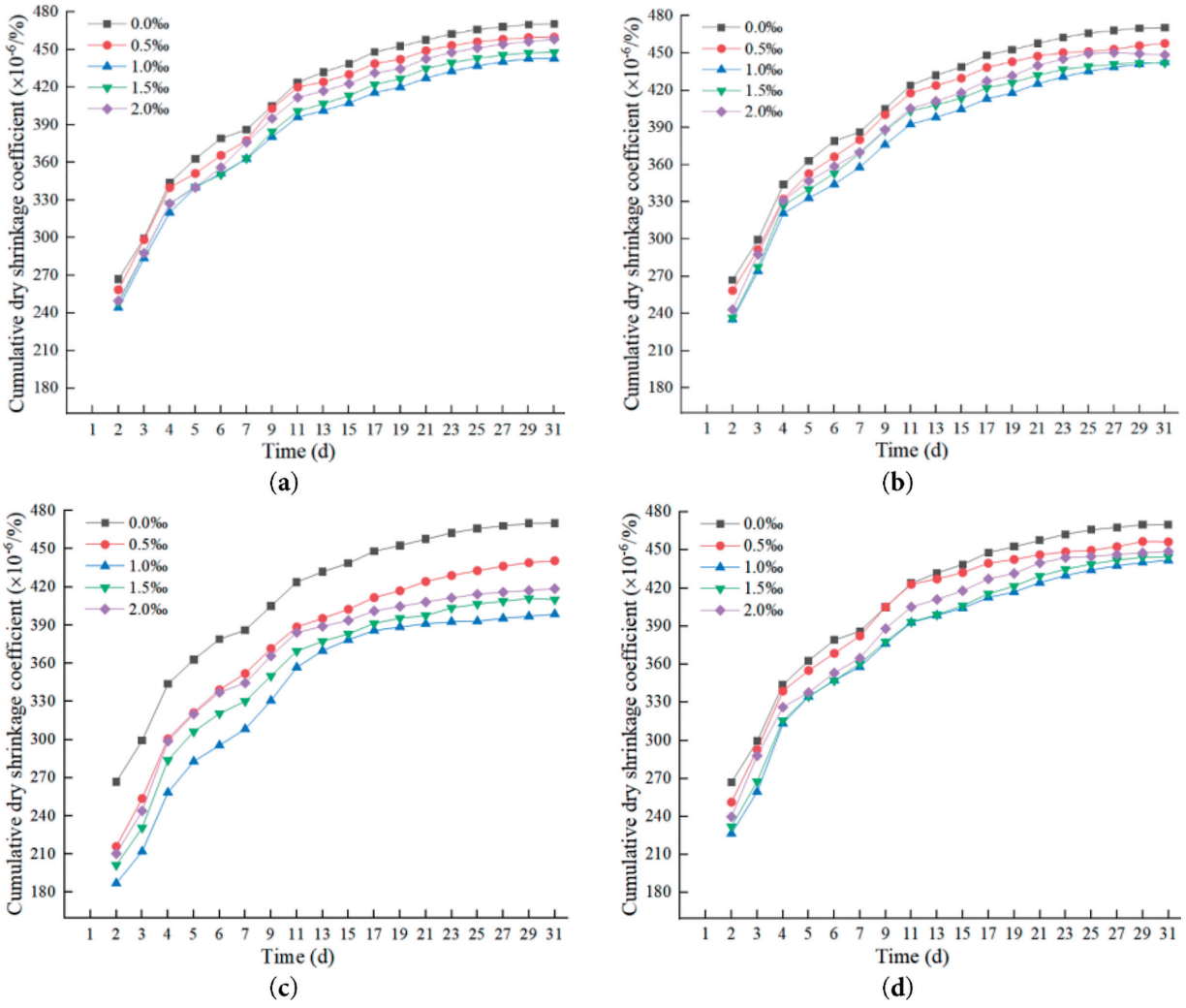

Figure 7 Cumulative dry shrinkage coefficient of basalt fiber cement stabilized sandstone gravel with different lengths; (a) 6 mm length basalt fiber; (b) 12 mm length basalt fiber; (c) 18 mm length basalt fiber; (d) 24 mm length basalt fiber. Note: The results of this experiment are the average of three groups of parallel experiments

$$\varepsilon_i = \frac{\delta_i}{l} \quad (2)$$

$$\alpha_{di} = \frac{\varepsilon_i}{w_i} \quad (3)$$

$$\alpha_d = \frac{\sum \varepsilon_i}{\sum w_i} \quad (4)$$

where, w_i is the i-th water loss rate (%); m_i is the i-th standard specimen weighing quality (g); m_p is the constant weight (g) of the standard specimen after drying; ε_i is the i-th drying shrinkage strain (10^{-6}); δ_i is the deformation of the i-th drying shrinkage displacement (mm); l is the length of the standard specimen (mm); α_{di} is the i-th drying shrinkage coefficient (10^{-6}/%); α_d is the total dry shrinkage coefficient (10^{-6}/%).

The test results indicate that the incorporation of basalt fiber improves the dry shrinkage performance of cement-stabilized sandstone gravel across various fiber lengths. Among the tested contents, 1.0% exhibited the most significant improvement, with the effectiveness of other contents ranked as follows: 2.0% > 1.5% > 0.5%. In terms of fiber length, 18 mm fibers provided the most notable enhancement, followed by 24 mm > 12 mm > 6 mm. Comprehensive analysis reveals that the combination of 18 mm fiber length and 1.0% content yields the optimal improvement, reducing the 31-day cumulative shrinkage coefficient by approximately 15% compared to the reference group. This enhancement is primarily attributed to the micro-mechanical effects generated by basalt fibers within the cement matrix. The strong interfacial bonding between fibers and aggregates effectively restrains drying shrinkage deformation. Meanwhile, the fibers exert a bridging effect at micro-cracks, delaying crack propagation and dispersing shrinkage stress. Compared to glass and Polyvinyl Alcohol (PVA) fibers [30, 31], basalt fiber possesses a higher elastic modulus and superior alkali resistance, enabling more durable and effective inhibition of dry shrinkage under the same conditions. The optimal performance of the 18 mm fiber length can be attributed to its good dispersibility during mixing and the formation of a fully continuous spatial network within the matrix. Short fibers offer a limited restraint range, whereas long fibers are prone to agglomeration and uneven distribution. Therefore, the 18 mm fiber achieves an optimal balance between crack bridging and uniform stress distribution.

The calculation formula of temperature shrinkage coefficient is shown in Equations (5) and (6), and the test results are shown in Figure 8.

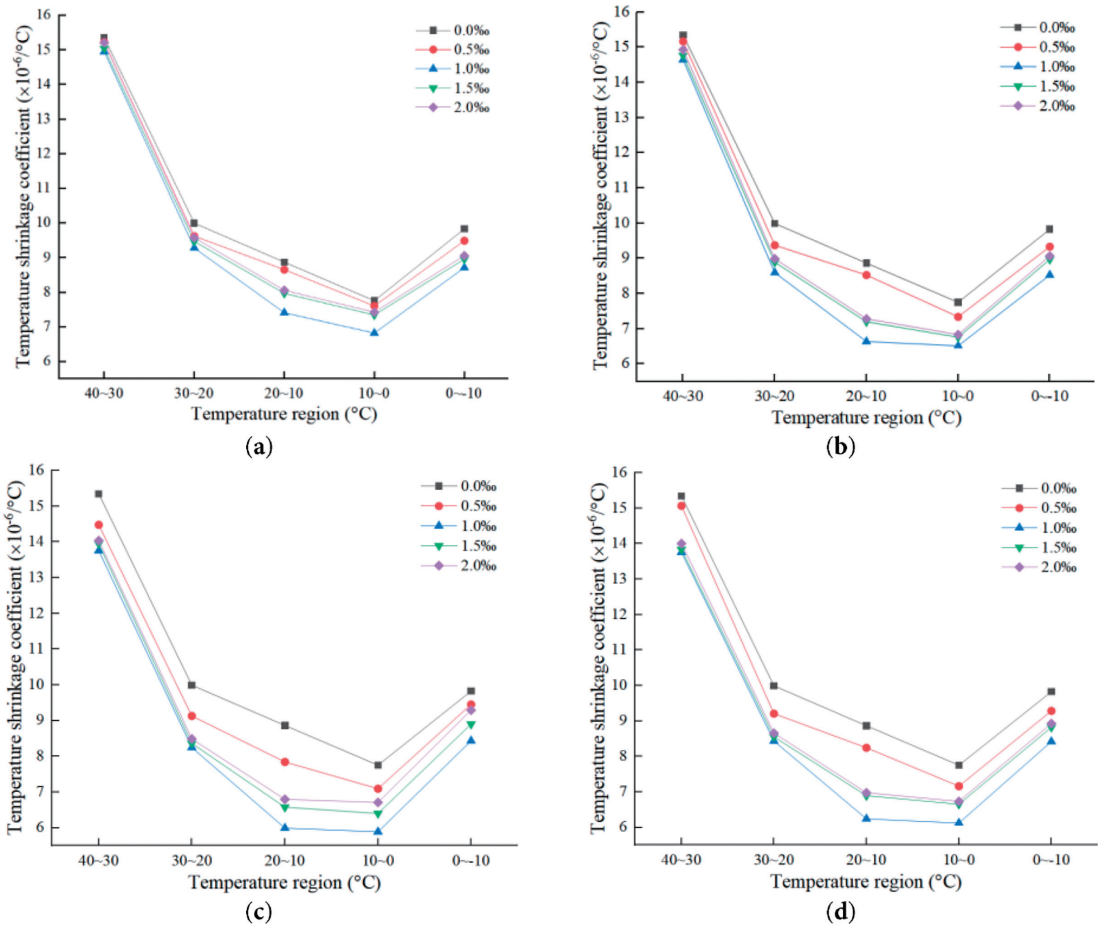

Figure 8 Temperature shrinkage coefficient of basalt fiber cement stabilized sandstone gravel with different lengths; (a) 6 mm length basalt fiber; (b) 12 mm length basalt fiber; (c) 18 mm length basalt fiber; (d) 24 mm length basalt fiber. Note: The results of this experiment are the average of three groups of parallel experiments

$$\varepsilon_i = \frac{l_i - l_{i+1}}{L_0} \quad (5)$$

$$\alpha_t = \frac{\varepsilon_i}{t_i - t_{i+1}} \quad (6)$$

where, ε_i is the average temperature shrinkage strain (10^{-6}) of the specimen in the *i*-th temperature range; l_i is the average value (mm) of the dial gauge reading in the *i*-th temperature range; L_0 is the initial length of the specimen (mm); α_i is the linear shrinkage coefficient of the material under unit temperature change (10^{-6}/°C); t_i is the *i*-th temperature range (°C) set by the temperature control program.

The test results show that the temperature shrinkage coefficient of cement-stabilized sandstone aggregate decreases first and then increases with the decrease in temperature. In the high temperature range (40–30°C), the temperature shrinkage coefficient reaches the maximum value, which is mainly due to the large internal stress caused by the differential thermal expansion between the cement paste and the aggregate. As the temperature drops to the normal low temperature range (30–0°C), the internal structure of the material tends to stabilize, the thermal stress is gradually released, and the temperature shrinkage coefficient decreases accordingly. In the negative temperature range (0 to −10°C), the volume expansion caused by the freezing of pore water and the tensile stress exerted by ice crystals on the pore walls leads to a renewed increase in the temperature shrinkage coefficient. The incorporation of basalt fiber can significantly improve the temperature shrinkage performance of the material. The mechanism is mainly reflected in the three-dimensional network structure formed by the fibers in the matrix, which can effectively restrain the temperature-induced shrinkage deformation and thus offset part of the thermal stress. The effect of fiber content on the improvement exhibits a clear trend of "first strengthening and then weakening": when the content is 1.0%, the fibers are uniformly dispersed, forming a continuous spatial support system, and the shrinkage inhibition effect is the best. When the content exceeds 1.0% (such as 1.5% and 2.0%), the fibers are prone to agglomeration, resulting in local stress concentration and weakening their overall restraining capacity, so the improvement effect tends to plateau or even decrease. The fibers with a length of 18 mm show the best inhibition effect, and the mechanism is that too short fibers (such as 6 mm) have a limited constraint range on the matrix and insufficient restraining ability, while too long fibers (such as 24 mm) are prone to entanglement during the mixing process, which affects the dispersion uniformity and interfacial bonding. Medium-length fibers (such as 18 mm) can effectively overlap in the matrix to form a stable three-dimensional framework and enhance the fiber-cement interfacial interaction, thereby better resisting temperature-induced deformation. Therefore, under the condition of 1.0% content and 18 mm fiber length, basalt fiber can construct a uniform and continuous three-dimensional network structure in cement-stabilized aggregate, maximize its bridging and crack resistance, significantly inhibit temperature shrinkage deformation, and improve the thermal stability of the material.

3.1.3 Computed Tomography (CT) scanning microscopic analysis of basalt fiber with different lengths and contents

In order to verify the difference in the microstructure of the mixture with different basalt fiber lengths and contents, CT scanning was performed on the mixture specimens with 5 different lengths and contents. The typical cross sections of cement stabilized macadam CT with different fiber content are shown in the Figure 9.

CT scanning images clearly reveal the influence of fiber length and content on the internal microstructure of cement-stabilized sandstone aggregate. Under the condition of 12 mm fiber length and 1% content, the specimen exhibits high internal porosity and distinct shrinkage cracks, indicating that this fiber parameter combination fails to form a continuous spatial network structure effectively. As a result, the fiber reinforcement provides limited restraint to the matrix, leading to the development of numerous microcracks during drying and temperature variations. In contrast, specimens with 18 mm fiber length and 1% content display a more uniform and dense microstructure, in which the fibers are well dispersed and form an effective three-dimensional supporting system, significantly reducing porosity and inhibiting the initiation and propagation of cracks. The 6 mm short fibers, due to their insufficient length, are unable to bridge microcracks effectively, offering only limited constraining capacity. On the other hand, 24 mm long fibers are prone to tangling during mixing, leading to localized fiber accumulation and pore concentration, which compromises the uniformity of the overall structure. Furthermore, under the condition of 18 mm length and 2% content, fiber agglomeration occurs easily, creating stress concentration points that weaken the integrity and reinforcing effect of the fiber network. Similarly, with 18 mm length and 0.5% content, the fiber distribution is insufficient to provide adequate stabilization, and shrinkage cracks remain evident. Comprehensive analysis confirms that basalt fibers with 18 mm length and 1% content construct an optimal fiber-matrix composite structure in cement-stabilized sandstone aggregate, effectively enhancing compactness and crack resistance, thereby corroborating the superior macroscopic mechanical

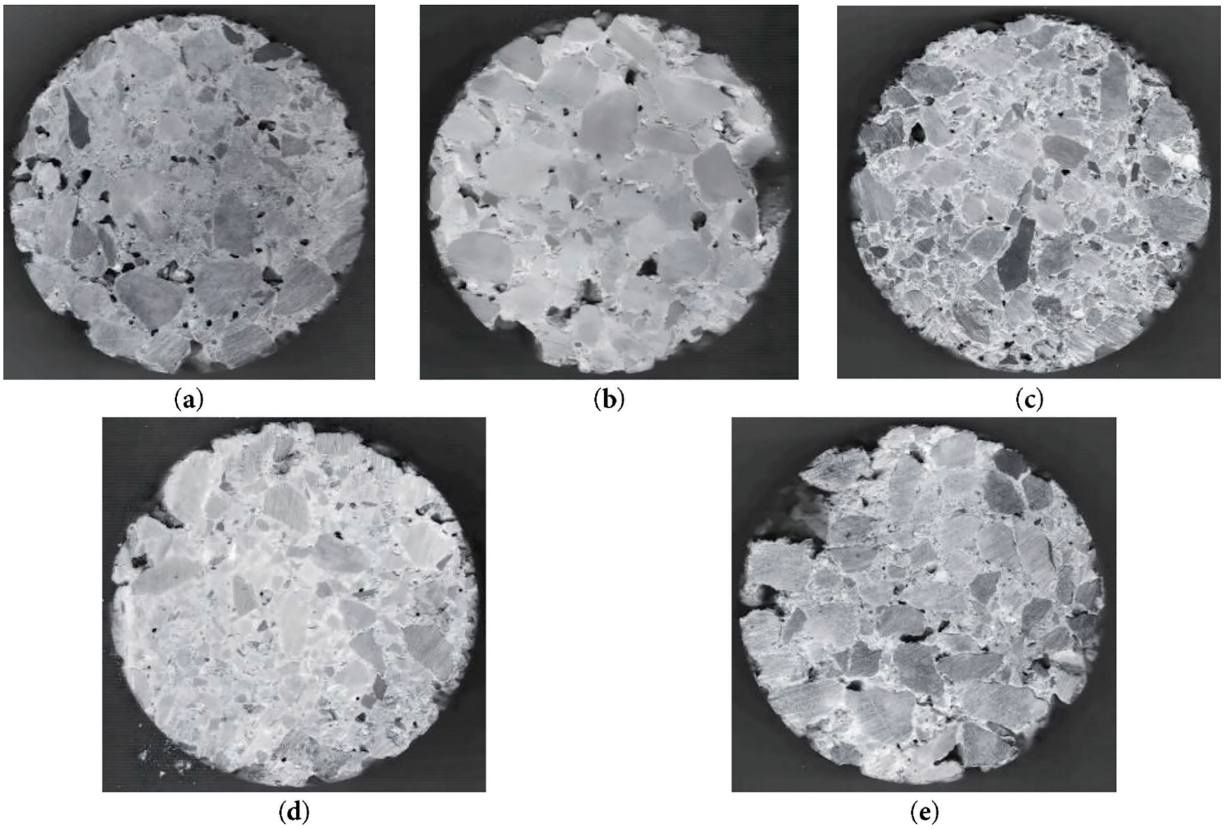

Figure 9 CT scan results of specimen section; (a) 6 mm, 1% dosage; (b) 18 mm, 0.5% dosage; (c) 18 mm, 1% dosage; (d) 24 mm, 1% dosage; (e) 18 mm, 2% dosage

and shrinkage properties from a microstructural perspective.

3.2 Strength characteristics of basalt fiber cement stabilized sandstone

3.2.1 Unconfined compressive strength test

Unconfined compressive strength tests were conducted on cylindrical specimens at standard curing ages of 7, 14, 28, 60, and 90 days to analyze the influence of curing age and basalt fiber on the strength development of cement-stabilized sandstone gravel. To facilitate clearer observation of the strength evolution trend, the maximum failure load P (in Newtons) was calculated using Equation (7). The coefficient of variation was determined in accordance with Equation (8). The representative value of unconfined compressive strength of the same group of tests is represented by R_d^0. According to the results of strength test, the representative value of strength is calculated according to Equation (9). The test results are shown in Figures 10 and 11.

$$R_c = \frac{P}{A} \tag{7}$$

$$C_v = \frac{S}{\overline{R}} \tag{8}$$

$$R_d^0 = \overline{R} \times \left(1 - Z_\alpha C_v\right) \tag{9}$$

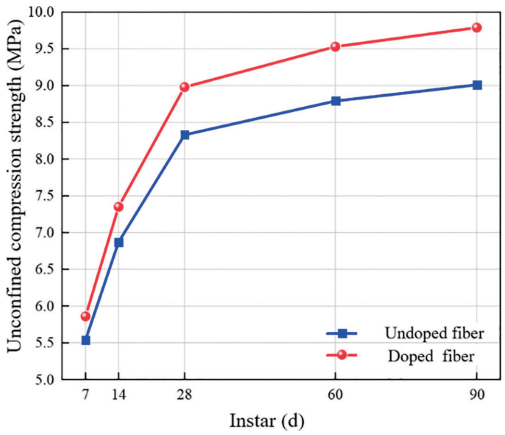

Figure 10 Growth law of unconfined compressive strength with age

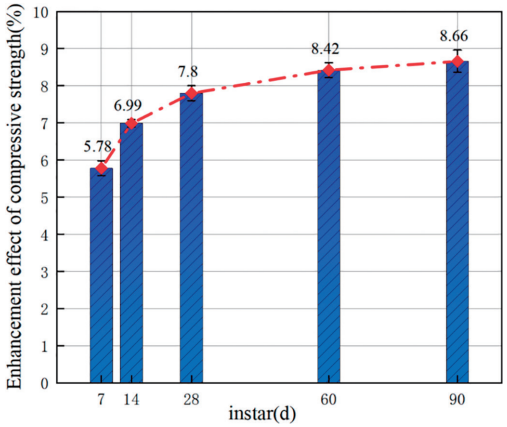

Figure 11 Effect of fiber on unconfined compressive strength improvement

where, R_c is the unconfined compressive strength (MPa) of the specimen; P is the maximum pressure (N) when the specimen is destroyed; A is the cross-sectional area (mm²) of the specimen. C_v is the coefficient of variation (%); S is the standard deviation; $\overline{R}$ is the average strength (MPa). R_d^0 is the representative value of strength (MPa); Z_α is the coefficient that varies with the guarantee rate or confidence α in the standard normal distribution table. Highways and first-class highways should take the guarantee rate of 95%, that is $Z_\alpha = 1.645$.

The test results indicate that the unconfined compressive strength of cement-stabilized sandstone gravel increases with curing age, with the most rapid growth occurring between 7 and 14 days, followed by the period from 14 to 28 days. The rate of strength gain slows from 28 to 90 days, eventually stabilizing. Without fiber reinforcement, the strength increased from 5.54 MPa at 7 days to 9.01 MPa at 90 days, which is attributed to the ongoing cement hydration leading to a denser microstructure and reduced porosity. At each curing age, the compressive strength of fiber-reinforced specimens exceeded that of the non-reinforced group, and the difference between the two became more pronounced over time. The percentage increase in strength due to fiber addition rose from 5.78% at 7 days to 8.66% at 90 days, indicating that while fiber contributed notably to early strength enhancement, its overall reinforcing effect became more substantial with prolonged aging. These results demonstrate that basalt fiber significantly improves the unconfined compressive strength of cement-stabilized sandstone gravel, and this improvement becomes more evident with extended curing duration.

3.2.2 Bending tensile strength test

Flexural tensile strength tests were conducted on beam specimens at standard curing ages of 7, 14, 28, 60, and 90 days. A comparison was made between the conventional flexural tensile strength and the value obtained when accounting for the difference in tensile and compressive moduli [32]. The formula for calculating flexural strength without considering the modulus difference is given in Equation (10), while the formulas for determining the flexural strength of cement-stabilized sandstone gravel incorporating the tensile-compressive modulus difference are provided in Equations (11)–(13). The test results of flexural strength considering the modulus difference, as well as the enhancing effect of fiber on flexural strength, are presented in Figures 12 and 13.

$$R_f = \frac{PL}{bh^2} \tag{10}$$

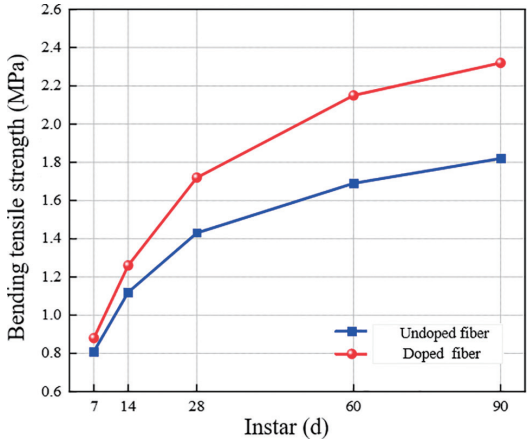

Figure 12 Growth law of flexural tensile strength with age

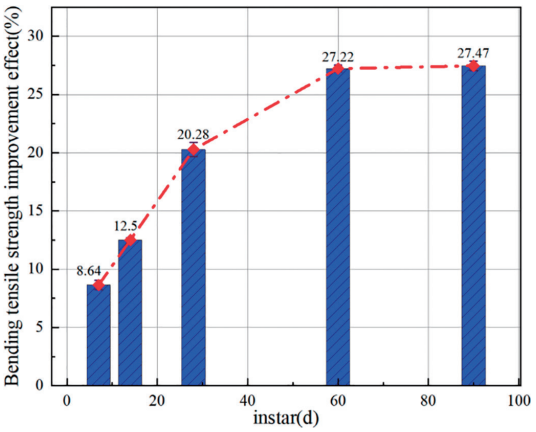

Figure 13 Effect of fiber on flexural strength improvement

Bottom layer tensile modulus:

$$E_t = \frac{PL(\varepsilon_t + \varepsilon_c)}{2bh^2\varepsilon_t^2} \tag{11}$$

Top pressure modulus:

$$E_c = \frac{PL(\varepsilon_t + \varepsilon_c)}{2bh^2\varepsilon_c^2} \tag{12}$$

Bending tensile strength considering the difference between tension and compression:

$$R_f^{'} = \frac{PL(\varepsilon_t + \varepsilon_c)}{2bh^2\varepsilon_t} \tag{13}$$

where, R_f is the flexural tensile strength (MPa); $R_f^{'}$ is the flexural tensile strength (MPa) considering the difference between tension and compression; P is the ultimate failure load (N); L is the span, the distance between the two fulcrums (mm); b is the width of the specimen (mm); h is the height of the specimen (mm); E_t is the bottom tensile modulus; E_c is the top pressure modulus;

ε_t is tensile strain at the bottom of the layer; ε_c is the top compressive strain.

The analysis results indicate that the flexural tensile strength of cement-stabilized sandstone gravel increases significantly with curing age, primarily due to the continuous hydration reaction of the cement. Without fiber reinforcement, the flexural strength increased from 0.81 MPa at 7 days to 1.82 MPa at 90 days. With the incorporation of fiber, the flexural tensile strength increased from 0.88 MPa to 2.32 MPa, demonstrating a more pronounced enhancement. The addition of fiber resulted in an 8.64% increase in flexural strength at 7 days, which further rose to 27.47% by 90 days. The inclusion of fibers markedly strengthened the material at all ages, and this improvement became more substantial over time. The fundamental mechanism of basalt fiber lies in its active intervention in and optimization of the material damage process. The mechanical essence of the three-dimensional network structure formed by the fibers within the material is the construction of an efficient stress transfer and redistribution system. When microcracks initiate, fibers bridging the cracks effectively transfer the locally concentrated stress to the uncracked regions of the matrix through interfacial bonding, thereby suppressing crack propagation and significantly enhancing the fracture toughness of the material. Additionally, this network structure improves the mechanical interlocking and synergistic interaction between aggregates and binders. From a mechanical perspective, the incorporation of fibers not only optimizes the internal stress distribution and mitigates local stress concentration, but also alters the failure mode of the material. This transformation enables the material to evolve from a brittle system into a composite system with enhanced toughness and stress redistribution capacity when subjected to bending and tensile loads, thereby achieving an essential improvement in flexural strength.

3.2.3 Direct tension test

Direct tensile strength tests were conducted on cylindrical specimens at standard curing ages of 7, 14, 28, 60, and 90 days to analyze the influence of curing age and basalt fiber on the direct tensile strength of cement-stabilized sandstone gravel. Fifteen parallel specimens were prepared for each group, and the mean value was calculated with the coefficient of variation (C_v) required to be ≤15%. The formula used for calculating direct tensile strength is given in Equation (14), and the test results are presented in Figures 14 and 15.

$$R_t = \frac{4P}{\pi d^2} \tag{14}$$

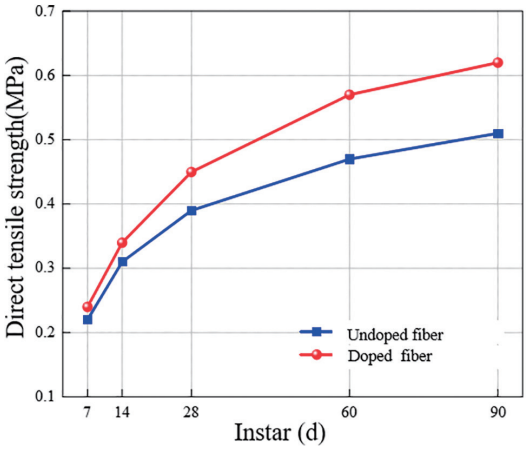

Figure 14 The growth law of direct tensile strength with age

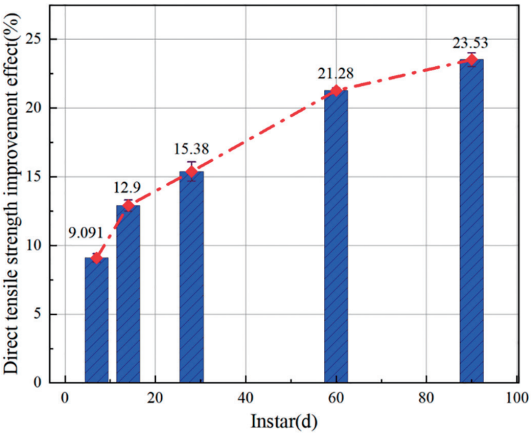

Figure 15 Effect of fiber on direct tensile strength improvement

where, R_t is the direct tensile strength (MPa); d is the diameter of the specimen (mm); P is the pressure (N) when the specimen is destroyed.

The test results indicate that the direct tensile strength of both non-fiber and fiber-reinforced cement-stabilized sandstone gravel continuously increases from 7 to 90 days of curing. The strength of non-reinforced specimens increased from 0.22 MPa to 0.51 MPa, while that of fiber-reinforced specimens rose from 0.24 MPa to 0.62 MPa. As the curing age extended, the hydration reaction led to a denser material structure, resulting in stabilized long-term strength. The incorporation of fiber resulted in higher direct tensile strength at each curing age compared to the non-reinforced specimens, and this difference became more pronounced over time. The strength improvement was 9.09% at 7 days and reached 23.52% by 90 days. The fibers form a stronger bond with the cement matrix, effectively restricting crack propagation, and this reinforcing effect becomes more significant with increasing curing age.

Figure 16 Dynamic water scouring test

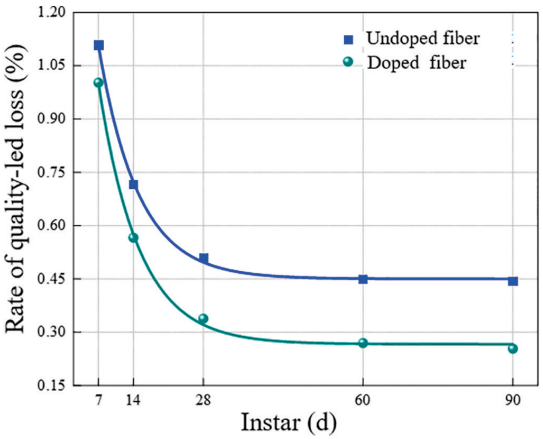

Figure 17 Mass loss rate of cement stabilized gravel at different ages

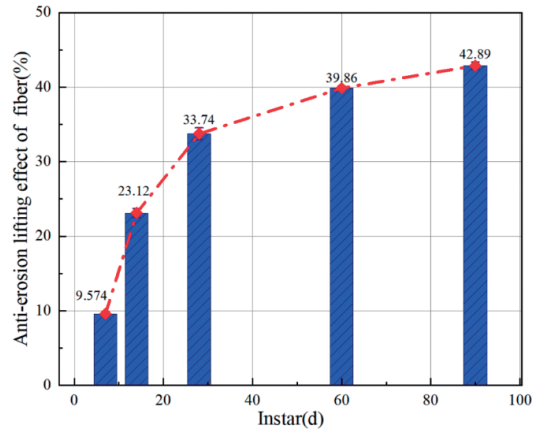

Figure 18 Anti-erosion effect of fiber on cement stabilized macadam

3.3 Study on erosion resistance characteristics of basalt fiber cement stabilized sandstone gravel

The cylindrical specimens with standard curing ages of 7 d, 14 d, 28 d, 60 d and 90 d were selected to carry out the dynamic water scour test, as shown in Figure 16. The anti-erosion effect index of fiber is used to characterize the anti-erosion effect of fiber on cement stabilized sandstone, see Equation (15). The test results are shown in Figures 17 and 18.

$$P_x = \frac{P_1 - P_2}{P_1} \times 100 \qquad (15)$$

where, P_x is the erosion resistance effect of basalt fiber cement stabilized sandstone gravel (%); P_1 and P_2 are the erosion mass loss rate (%) of cement stabilized sandstone gravel without and with fiber, respectively.

The test results demonstrate that the erosion resistance performance of cement-stabilized sandstone gravel improves significantly with increasing curing age, accompanied by a decrease in the eroded mass loss rate. Without fiber addition, the eroded mass decreased from 68.73 g at 7 days to 27.56 g at 90 days, and the mass loss rate decreased from 1.11% to 0.44%. With fiber incorporation, the eroded mass was reduced from 62.15 g to 15.74 g, and the mass loss rate decreased from 1.00% to 0.25%. At each curing age, both the eroded mass and the mass loss rate of the fiber-reinforced specimens were lower than those of the non-reinforced specimens. Moreover, the improvement in anti-erosion performance due to fiber addition became more pronounced with prolonged curing age.

The cement hydration reaction plays a key role in enhancing erosion resistance. As the curing age increases, the growing amount of cement

hydration products fills the pores, resulting in a denser material structure and reduced porosity. This decrease in pore space limits water infiltration pathways, thereby slowing down the rate of erosion-induced damage. Simultaneously, the increased hydration products improve the overall strength of the material. The incorporation of basalt fibers forms a three-dimensional reinforcing network within the matrix, which blocks the direct impact of water flow on solid particles, dissipates hydraulic energy, fills micro-pores, further reduces porosity, and limits the penetration of water flow.

4 Conclusion

To make the sandstone graded crushed stone better applied to road construction, this paper incorporated basalt fiber into sandstone graded crushed stone, and carried out erosion resistance and strength tests. The mechanical properties of basalt fiber reinforced cement stabilized sandstone crushed stone were systematically studied. The main conclusions are as follows:

1. The influence of fiber length and content on shrinkage performance exhibits a notable threshold effect and size dependence. The spatial network structure formed by 18 mm fibers in the matrix is optimal, as it ensures sufficient anchorage length while avoiding the agglomeration tendency associated with excessively long fibers. A content of 1.0% enables the formation of an effective three-dimensional reinforcement network without compromising the workability of the mixture. This study elucidates the interaction mechanism at the fiber–aggregate–cement matrix multiphase interface from a micromechanical perspective, revealing the synergistic "bridging–force–crack resistance" effect of fibers in high-porosity sandstone. These findings provide a theoretical basis for the fiber-reinforced design of weakly acidic aggregates.
2. Basalt fiber enhances the shrinkage performance of cement-stabilized sandstone aggregate through multiple physical mechanisms. The reduction in the drying shrinkage coefficient results from the dispersive effect of fibers on capillary tension and shrinkage stress. The improvement in temperature shrinkage performance is attributed to the constraining effect of the fiber network on thermal strain, particularly in the ambient temperature range (30–0°C), where the temperature shrinkage coefficient is reduced by 32.4%. This confirms that the fiber contributes most significantly during the shrinkage stage dominated by the cement paste. These findings provide a scientific basis for guiding anti-cracking design of pavements in different temperature zones and overcoming the technical limitation of traditional shrinkage control methods that rely solely on reducing cement content.
3. The combined effect of basalt fiber and curing age significantly enhances the scouring resistance of cement-stabilized sandstone aggregate. With the incorporation of fiber, the mass loss rate at 90 days of curing age decreases from 0.44% to 0.25%. The fiber mitigates overall damage in the cement-stabilized aggregate through a "mass–strength synergistic protection mechanism." The three-dimensional network formed by the fibers not only directly hinders water infiltration but also refines the pore structure, thereby reducing penetration paths. Simultaneously, the fiber–aggregate interfacial interaction enhances the bonding force between aggregates and the cementitious binder, further improving durability.
4. The design method for basalt fiber-reinforced sandstone cement-stabilized gravel material proposed in this study offers a technically feasible solution for highway construction in sandstone-rich regions such as Guangxi, China, with considerable potential for resource substitution and cost reduction. By optimizing the fiber blending process, it is possible to significantly decrease material and transportation costs while achieving comprehensive enhancement of base course performance, demonstrating promising potential for engineering applications.

Acknowledgement

The authors express gratitude to Dr. Xinglong Gao for the ideas he provided for the research framework and the contributions he made in the research process.

Funding Statement

This research was funded by the Key Scientific Research Project of Hunan Provincial Department of Education of Funder, grant number 23A0246, and Key Scientific and Technological Projects in the Transportation Industry (Resource Utilization Technology of Sandstone in Guangxi High-Grade Highway Pavement Engineering) of Funder, grant number 22MS5125.

Author Contributions

Conceptualization, Bin Zhang; methodology, Bin Zhao; software, Zhanli Zhang; validation, Bin Zhang, Bin Zhao, Zhanli Zhang, Yongliang Liu, Tuo Huang and Dabin Zhang; formal analysis, Yongliang Liu; investigation, Tuo Huang; resources, Bin Zhang; data curation, Dabin Zhang; writing—original draft preparation, Bin Zhang; writing—review and editing, Bin Zhao; visualization, Zhanli Zhang; supervision, Yongliang Liu; project administration, Tuo Huang; funding acquisition, Dabin Zhang. All authors reviewed the results and approved the final version of the manuscript.

Availability of Data and Materials

The data that support the findings of this study are available from the corresponding author, Zhanli Zhang, upon reasonable request.

Ethics Approval

Not applicable.

Conflicts of Interest

The authors declare no conflicts of interest to report regarding the present study.

REFERENCES

[1] Liu P, Li B, Guo F, Wu X, Yao T. Study on refined crushing technology of RAP and mechanical properties of RAP-doped cement-stabilised macadam base. Materials. 2025;18(1):147. doi:10.3390/ma18010147.

[2] Li Q, Chen Z. Numerical analysis and conversion of dynamic and static deflection of asphalt pavement under FWD loading. Constr Build Mater. 2023;367(3):129513. doi:10.1016/j.conbuildmat.2022.129513.

[3] Chai GW, van Staden R, Loo YC. *In situ* assessment of pavement subgrade using falling weight deflectometer. J Test Eval. 2015;43(1):140–8. doi:10.1520/jte20130149.

[4] Bilema M, Yuen CW. Viability of using high reclaimed asphalt pavement (RAP) contents incorporating waste materials for eco-friendly paving applications: a systematic review. Environ Sci Pollut Res. 2025;32(26):15493–517. doi:10.1007/s11356-025-36614-x.

[5] Shi L, Guo H, Zeng G, Zhou R, Li X, Lin B, et al. Key parameters and effects in image processing and aggregate-aggregate contact calculation of asphalt mixtures. Measurement. 2025;239(1):115439. doi:10.1016/j.measurement.2024.115439.

[6] Shi L, Liang H, Wang D, Liu T. Mesogenetic evaluation and design of coarse aggregate contact within asphalt mixture. J Mater Civ Eng. 2022;34(8):04022187. doi:10.1061/(asce)mt.1943-5533.0004344.

[7] Liang H, Guo H, Zhang J, Li H, Shi L, Deng K. Influence of gradation composition on crack evolution of stone mastic asphalt based on digital image processing. Theor Appl Fract Mech. 2025;136(7):104848. doi:10.1016/j.tafmec.2025.104848.

[8] Yuan Y, Hu X, Wang K, Liu Z, Zhong M, Meng K. Study on mechanical properties of road cement-stabilized macadam base material prepared with construction waste recycled aggregate. Buildings. 2024;14(9):2605. doi:10.3390/buildings14092605.

[9] Yi Y, Jiang Y, Ouyang L, Zhang Y, Tian T, Fan J, et al. Maximizing the utilization of construction waste in cement-stabilized macadam based on mechanics and durability performance. Constr Build Mater. 2025;473(11):141089. doi:10.1016/j.conbuildmat.2025.141089.

[10] Kong D, Zou J, Chen M, Xie J, Gou X. Sustainable application of pyrolytic oxygen furnace slag in cement-stabilized macadam: volume stability, mechanical properties, and environmental impact. Sustainability. 2024;16(10):3965. doi:10.3390/su16103965.

[11] Li W, Lang L, Lin Z, Wang Z, Zhang F. Characteristics of dry shrinkage and temperature shrinkage of cement-stabilized steel slag. Constr Build Mater. 2017;134(10):540–8. doi:10.1016/j.conbuildmat.2016.12.214.

[12] Yuan L, Liu L, He M, Liu Q, Cheng H, Sun L, et al. Sustainable pavement solutions: performance enhancement using high-dosage unequal-sized feldspar powder as a replacement for natural aggregates in cement stabilized macadam bases. Constr Build Mater. 2025;459(03):139620. doi:10.1016/j.conbuildmat.2024.139620.

[13] Du Q, Pan T, Lv J, Zhou J, Ma Q, Sun Q. Mechanical properties of sandstone cement-stabilized macadam. Appl Sci. 2019;9(17):3460. doi:10.3390/app9173460.

[14] Kumar S, Gupta RC, Shrivastava S. Strength, abrasion and permeability studies on cement concrete containing quartz sandstone coarse aggregates. Constr Build Mater. 2016;125:884–91. doi:10.1016/j.conbuildmat.2016.08.106.

[15] Liao Y, Lv Y, Huang G, Ren S, Wang XY, Guo R, et al. Strength and microstructure analysis of subgrade materials containing red sandstone-limestone-cement composites and red sandstone gravel. Constr Build Mater. 2024;416:135190. doi:10.1016/j.conbuildmat.2024.135190.

[16] Chen J, Zhu Z, Zhou L, Ma L, Wang H, Wang M. Failure mechanism analysis and tensile constitutive model of basalt fiber concrete-rock interface based on fiber surface modification. Compos Struct. 2024;338(2):118110. doi:10.1016/j.compstruct.2024.118110.

[17] Heirani P, Mahmoudi S, Shalchian MM, Zanganeh Ranjbar P, Arabani M, Salimi M, et al. Eco-friendly approach to clay stabilization: integrating carbide lime, steel slag, and tire textile waste. J Mater Res Technol. 2025;39:2718–41. doi:10.1016/j.jmrt.2025.10.022.

[18] Pouramin M, Payan M, Salimi M, Ashournia M, Zanganeh Ranjbar P, Saeidi A. Rapid stabilization of highly expansive clays: synergistic approach with polyurethane and waste tire textile fiber for enhanced mechanical properties. J Mater Civ Eng. 2025;37(11):04025397. doi:10.1061/jmcee7.mteng-19917.

[19] Guo Y, Liu Y, Shen A, Li Z, Wu J, Zhang J. Research on shrinkage and softening crack resistance of glass fiber cement stabilized macadam. J Zhengzhou Univ Eng Sci. 2023;44(5):114–20. (In Chinese). doi:10.13705/j.issn.1671-6833.2023.02.016.

[20] Zhao Y, Yang X, Zhang Q, Liang N, Xiang Y, Qin M. Crack resistance and mechanical properties of polyvinyl alcohol fiber-reinforced cement-stabilized macadam base. Adv Civ Eng. 2020;2020(1):6564076. doi:10.1155/2020/6564076.

[21] Li X, Lv X, Wang W, Liu J, Yu M, You Z. Crack resistance of waste cooking oil modified cement stabilized macadam. J Clean Prod. 2020;243(4):118525. doi:10.1016/j.jclepro.2019.118525.

[22] Zheng Y, Zhang P, Cai Y, Jin Z, Moshtagh E. Cracking resistance and mechanical properties of basalt fibers reinforced cement-stabilized macadam. Compos Part B Eng. 2019;165(4):312–34. doi:10.1016/j.compositesb.2018.11.115.

[23] Branston J, Das S, Kenno SY, Taylor C. Influence of basalt fibres on free and restrained plastic shrinkage. Cem Concr Compos. 2016;74(11):182–90. doi:10.1016/j.cemconcomp.2016.10.004.

[24] Shao J, Ma J, Liu R, Liu Y, Zhang P, Tang Y, et al. Experimental investigation on fracture performance of short basalt fiber bundle reinforced concrete. Struct Durab Health Monit. 2022;16(4):291–305. doi:10.32604/sdhm.2022.015097.

[25] Qin S, Wu L. Study on mechanical properties and mechanism of new basalt fiber reinforced concrete. Case Stud Constr Mater. 2025;22(5):e04290. doi:10.1016/j.cscm.2025.e04290.

[26] JTG/T F20-2015. Highway pavement base construction technical rules. Beijing, China: Ministry of Transport of China; 2015. (In Chinese).

[27] JTG 3441-2024. Test procedure for inorganic binder stabilized materials of highway engineering. Beijing, China: Ministry of Transport of China; 2024. (In Chinese).

[28] JTG D50-2017. Highway pavement base construction technical rules. Beijing, China: Ministry of Transport of China; 2017. (In Chinese).

[29] Khan M, Cao M. Effect of hybrid basalt fibre length and content on properties of cementitious composites. Mag Concr Res. 2021;73(10):487–98. doi:10.1680/jmacr.19.00226.

[30] Yang Z, Yu F, Li X. Effect of surface modification methods on the properties of recycled glass fiber cementitious composites. Chem Eng Sci. 2025;303(17):120973. doi:10.1016/j.ces.2024.120973.

[31] Arain MF, Wang M, Chen J, Zhang H. Study on PVA fiber surface modification for strain-hardening cementitious composites (PVA-SHCC). Constr Build Mater. 2019;197(471):107–16. doi:10.1016/j.conbuildmat.2018.11.072.

[32] Huang T, Yu X, Lin B, Zhou L, Qian G, Wang Z. Fatigue residual strength and damage evolution of asphalt mixture under different stress states. Chin J Highw. 2024;37(12):284–93. (In Chinese). doi:10.19721/j.cnki.1001-7372.2024.12.010.